Acta Pharmacologica Sinica

www.nature.com/aps

ARTICLE

# Puerarin-V prevents the progression of hypoxia- and monocrotaline-induced pulmonary hypertension in rodent models

Di Chen[1,2], Hui-fang Zhang[1,2], Tian-yi Yuan[1,2], Shu-chan Sun[1,2], Ran-ran Wang[1,2], Shou-bao Wang[1,2], Lian-hua Fang[2], Yang Lyu[1,3] and Guan-hua Du[1,2]

Pulmonary hypertension (PH) is a cardiopulmonary disease characterized by a progressive increase in pulmonary vascular resistance. One of the initial pathogenic factors of PH is pulmonary arterial remodeling under various stimuli. Current marketed drugs against PH mainly relieve symptoms without significant improvement in overall prognosis. Discovering and developing new therapeutic drugs that interfere with vascular remodeling is in urgent need. Puerarin is an isoflavone compound extracted from the root of *Kudzu vine*, which is widely used in the treatment of cardiovascular diseases. In the present study, we evaluated the efficacy of puerarin in the treatment of experimental PH. PH was induced in rats by a single injection of MCT (50 mg/kg, sc), and in mice by exposure to hypoxia (10% $O_2$) for 14 days. After MCT injection the rats were administered puerarin (10, 30, 100 $mg \cdot kg^{-1} \cdot d^{-1}$, i.g.) for 28 days, whereas hypoxia-treated mice were pre-administered puerarin (60 $mg \cdot kg^{-1} \cdot d^{-1}$, i.g.) for 7 days. We showed that puerarin administration exerted significant protective effects in both experimental PH rodent models, evidenced by significantly reduced right ventricular systolic pressure (RVSP) and lung injury, improved pulmonary artery blood flow as well as pulmonary vasodilation and contraction function, inhibited inflammatory responses in lung tissues, improved resistance to apoptosis and abnormal proliferation in lung tissues, attenuated right ventricular injury and remodeling, and maintained normal function of the right ventricle. We revealed that MCT and hypoxia treatment significantly downregulated BMPR2/Smad signaling in the lung tissues and PPARγ/PI3K/Akt signaling in the lung tissues and right ventricles, which were restored by puerarin administration. In addition, we showed that a novel crystal type V (Puer-V) exerted better therapeutic effects than the crude form of puerarin (Puer). Furthermore, Puer-V was more efficient than bosentan (a positive control drug) in alleviating the abnormal structural changes and dysfunction of lung tissues and right ventricles. In conclusion, this study provides experimental evidence for developing Puer-V as a novel therapeutic drug to treat PH.

**Keywords:** pulmonary hypertension; vascular function; pulmonary arterial remodeling; right ventricular remodeling; puerarin; Puer-V

*Acta Pharmacologica Sinica* (2022) 43:2325–2339; https://doi.org/10.1038/s41401-022-00865-y

## INTRODUCTION

Pulmonary hypertension (PH) is a cardiopulmonary disease characterized by a progressive increase in pulmonary vascular resistance, accompanied by a continuous increase in pulmonary artery pressure and right ventricular systolic pressure (RVSP) and a decrease in cardiac output. All forms of PH affect nearly 1% of the global population, and approximately 10% of people over 65 years are affected [1]. According to the 6th World Symposium on Pulmonary Hypertension, a mean pulmonary arterial pressure greater than 20 mmHg is set as the clinical diagnostic criterion [2]. Pulmonary arterial remodeling is the pathogenic hallmark of all forms of pulmonary hypertension, which is a major condition with no currently available marketed drugs. Secondary to elevated pulmonary artery pressure, right ventricular hypertrophy and remodeling are the major causes of death. Currently, marketed drugs against PH mainly target three pathways: the endothelin-1 (ET-1), nitric oxide, and prostacyclin pathways [3] which are involved in the control of pulmonary vasomotor tone and vascular cell proliferation [4]. However, these therapies mainly relieve symptoms without significant improvement in overall prognosis. Therefore, identification of a novel drug that can improve pulmonary arterial remodeling and right ventricular remodeling for the treatment of PH is urgently needed.

According to the widely accepted international standards, there are five different types of PH based on the cause of disease [2]. It is widely applied for pharmacodynamic evaluation using a rat model

[1]State Key Laboratory of Bioactive Substances and Functions of Natural Medicines, Institute of Materia Medica, Chinese Academy of Medical Sciences and Peking Union Medical College, Beijing 100050, China; [2]Beijing Key Laboratory of Drug Targets Identification and Drug Screening, Institute of Materia Medica, Chinese Academy of Medical Sciences and Peking Union Medical College, Beijing 100050, China and [3]Beijing Key Laboratory of Polymorphic Drugs, Institute of Materia Medica, Chinese Academy of Medical Sciences and Peking Union Medical College, Beijing 100050, China
Correspondence: Lian-hua Fang (fanglh@imm.ac.cn) or Yang Lyu (luy@imm.ac.cn) or Guan-hua Du (dugh@imm.ac.cn)
These authors contributed equally: Di Chen, Hui-fang Zhang, Tian-yi Yuan

Received: 6 September 2021 Accepted: 9 January 2022
Published online: 21 February 2022

of monocrotaline (MCT)-induced pulmonary arterial hypertension (PAH) [5] and a mouse model of hypoxia-induced hypoxic pulmonary hypertension (HPH) mice model [6]. PAH belongs to the first category and HPH belongs to the third category. The mechanism by which MCT induces PH involves the liver metabolites of MCT damaging the pulmonary arterial endothelium, inducing vascular remodeling, and subsequently increasing vascular resistance. It is widely used in preclinical studies for drug development and mechanistic research for PAH. Hypoxia induces PH because a low oxygen concentration induces abnormal contraction and remodeling of the pulmonary artery and increases pulmonary vascular resistance, which contributes to the development of HPH [7]. Both models can commendably simulate the pathological process of pulmonary hypertension.

Puerarin (7,4-dihydroxy-8-β-*D*-glucosyl isoflavone, $C_{21}H_{20}O_9$, Fig. 1) [8] is extracted from the root of the Chinese herb *Kudzu vine*, and is widely used to clinically treat cardiovascular and cerebrovascular diseases, including myocardial infarction, cerebral ischemia, angina pectoris, and hypertension in China and other Asian countries [9]. Studies have shown that puerarin has protective effects on blood vessels and the myocardium, and can even restore pulmonary artery function and inhibit vascular remodeling to a certain extent. Puerarin has poor water solubility and fat solubility, which contribute to its low gastrointestinal absorption and bioavailability. Therefore, puerarin is mainly administered by clinical injection. Clinical trials have found that long-term use of injections will cause drug accumulation and hemolysis, and produce toxic effects. After crystal modification, five types of crystal forms of puerarin were obtained. Among them, the crystal V-type of puerarin (Puer-V) showed better gastrointestinal absorption and bioavailability than other crystal forms [8]. Therefore, Puer-V was used to evaluate its therapeutic effect on PH and its underlying mechanism in the present study.

## MATERIALS AND METHODS

### Materials

Puer-V is an optimal drug crystal modified by the Institute of Materia Medica, Chinese Academy of Medical Sciences (purity >99%). Unless otherwise stated, all other reagents were purchased from Sigma–Aldrich (St. Louis, MO, USA). Primary antibody against β-actin was obtained from Proteintech Group (Rosemont, IL, USA). Other primary antibodies were purchased from Cell Signaling Technology (Beverly, MA, USA).

### Animals and ethics

For the evaluation of the therapeutic effect of puerarin against MCT-induced pulmonary arterial hypertension, male Sprague-Dawley rats ($n = 105$, 170–190 g) were purchased from the Institute of Laboratory Animals Sciences, Chinese Academy of Medical Sciences, Beijing, China. For the evaluation of the therapeutic effect of puerarin against hypoxic pulmonary hypertension, male C57BL/6J mice ($n = 50$, 19–21 g) were purchased from Vital River Laboratories, Beijing, China. Animal care and handling were approved by the Animal Ethics Committee of the Chinese Academy of Medical Science and Peking Union Medical College.

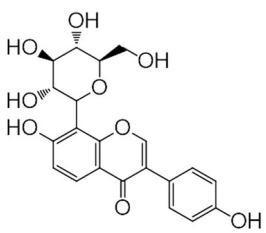


**Fig. 1 The chemical structure of puerarin.** Puerarin: 7,4-dihydroxy-8-β-*D*-glucosyl isoflavone; $C_{21}H_{20}O_9$, $M_w$, 416.38.

### Establishment of the rat model of MCT-induced PAH and hemodynamic measurements

Rats with similar baseline characteristics were randomly divided into 7 groups ($n = 15$ per group): control group, model group, bosentan (30 mg/kg) + MCT group, Puer-V low, medium and high dose groups (10, 30, 100 mg/kg) with MCT injection, and the crude form of puerarin (Puer) (30 mg/kg) + MCT group. Model establishment was performed by a single subcutaneous injection of MCT (50 mg/kg), whereas animals in the control group were subcutaneously injected with the same volume of normal saline. Bosentan (30 mg/kg, suspended in 0.5% CMC-Na), Puer-V (10, 30, 100 mg/kg, in solid form), and Puer (30 mg/kg, suspended in 0.5% CMC-Na) were orally administered every day for 28 days beginning on the 1st day after MCT injection. The control and model groups received the same volume of saline. On the 28th day, rats were killed for experimental end point detection. After rats in each group were anesthetized by an intraperitoneal injection of pentobarbital sodium (40 mg/kg), relevant hemodynamic indicators were tested. The RVSP was measured through the external carotid vein using a polyethylene-50 catheter with a BL-420S biological function experimental system (Chengdu Techman, China). Echocardiography measurements were performed by an echocardiogram system using a 17-MHZ transducer (Visual Sonic, Canada). On the parasternal short-axis view at the aortic level, Doppler-mode recording through the pulmonary artery and right ventricle was used to assess the pulmonary velocity profile and the structure of the right ventricle. The time from the onset of pulmonary outflow to maximal flow (pulmonary artery acceleration time, PAAT), maximum pulmonary velocity ($PV_{max}$) and pulmonary artery blood flow velocity time integral (PA VIT) were measured [10]. For the analysis of the structure and function of the right ventricle, right ventricle wall thickness, right ventricle cavity width, right ventricular output, and right ventricular stroke volume were measured.

### Whole blood collection and serum NT-proBNP and cTnT detection

Once hemodynamic indicators were collected, whole blood was collected through the abdominal aorta. After coagulation for 1 h at room temperature, the whole blood was centrifuged for 15 min at 5000 r/min at 4 °C for serum collection. The concentrations of N-terminal pro brain natriuretic peptide (NT-proBNP) and cardiac troponin T (cTnT) (Cusabio, Wuhan, China) were detected by ELISA kits according to the manufacturer's instructions.

### Evaluation of pulmonary artery function in vitro

After the blood was collected, secondary pulmonary arteries of rats in different groups were dissected and cut into 3–4 mm rings for pulmonary artery function assessment. After the rings were equilibrated for 10 min, the activity of the rings was tested by a high potassium (60 mM) solution [11]. Rings with increased tension of more than 1 g force could be used for further investigation. Then the contractibility of the rings was evaluated by the degree of contraction after adding 1 μM phenylephrine (Phe) and 0.01 μM ET-1 to the rings. The degree of contraction is expressed as the proportion of rings stimulated by the high potassium solution. After elution to baseline, the rings were preconstricted with 1 μM phenylephrine. Then 0.01–100 μM acetylcholine (ACh) or sodium nitroprusside (SNP) was added in concentration gradient to the bath. The diastolic function of the rings was reflected by the relaxation that ACh or SNP could produce in the rings.

### Tissue isolation

Once whole blood was collected, the rats were euthanized and the heart and lung were harvested for organ index measurement.

The weights of the whole heart, lung, whole ventricle, and right ventricle were recorded. The lung index was calculated by the weight ratio of the lung to the whole body. The right ventricular hypertrophy index was calculated by the weight ratio of the right ventricle to the interventricular septal plus left ventricle. In some separate experiments, the inferior lobe of the left lung and right ventricle was fixed in 4% paraformaldehyde and then embedded in paraffin and sectioned for immunohistochemical analysis. The lung tissue sections were stained with hematoxylin and eosin (H&E) and CD68 for morphological analysis and analysis of inflammation. For the wall thickness percentage calculation of different diameters of pulmonary arteries, elastic van Gieson [11] staining was used on the lung tissue sections. The right ventricular sections were stained with H&E, Masson and CD31 for morphological analysis, collagen deposition detection, and vascular density observation.

### Detection of the expression levels of ET-1 and inflammatory factors in lung tissues

Lung tissues were homogenized and then centrifuged at 12,000 × *g* at 4 °C for 20 min. The supernatant was obtained for subsequent detection. The concentrations of ET-1 and the inflammatory factor IL-6 were detected by ELISA kits according to the manufacturer's instructions. The expression levels of these factors were normalized to the protein content of the corresponding samples.

### Establishment of the mouse model of HPH and efficacy evaluation

Fifty male C57BL/6J mice were randomly divided into 5 groups ($n = 10$ per group): normoxia group, hypoxia group, hypoxia +sildenafil (30 mg/kg) group, hypoxia+Puer-V (60 mg/kg) group and hypoxia+Puer (60 mg/kg) group. The drugs were administered 7 days before model establishment. Mice were placed in a normobaric chamber and exposed to hypoxia (10% $O_2$) or normoxia (20% $O_2$) for 14 days. The body weight of mice in different groups was recorded every 4 days during the experiment. At the end of the experiment, the mice were examined for walking capacity by running on a treadmill. After the treadmill test, the mice were anesthetized with 200 mg/kg tribromoethanol to measure the RVSP using a Millar catheter-transducer (Millar Instruments, USA). Once hemodynamic data were collected, the mice were euthanized, and the hearts, lungs, and spleens were harvested and weighed. The right ventricular hypertrophy index and organ index were determined by the same method described in the 'Tissue isolation' section.

### Evaluation of the cytotoxicity and proliferation inhibitory effect of Puer-V

HPASMCs were obtained from ScienCell company (Carlsbad, USA) and cultured in Dulbecco's modified of Eagle's medium (DMEM) supplemented with 10% fetal bovine serum. Cells between the 3rd and 9th passages were used for the experiment. HPASMCs were cultured in an incubator containing 5% $CO_2$ and kept at 37 °C. To study the influence of Puer-V on HPASMC proliferation induced by hypoxia, we seeded 5000 cells per well in 96-well plates. Evaluation of the cytotoxicity of Puer-V was assessed by the viability of HPASMCs after treatment with different concentrations of Puer-V for 48 h. Cell proliferation detection was performed as follows. After 24 h of culture, the medium was replaced with serum-free medium to let the cells undergo growth arrest and treated with 3, 10, and 30 μM Puer-V for 48 h. Cell viability was determined by a CCK-8 kit (Dojindo, Japan) after culture under hypoxic (1% $O_2$) or normoxic (20%) conditions with or without Puer-V treatment.

### Detection of ROS formation in HPASMCs induced by hypoxia

HPASMCs were seeded in black 96-well plates with clear bottoms at a density of $5 \times 10^4$ cells/mL. The process of cell culture, cell growth arrest and Puer-V administration was the same as above. After 48 h of incubation in a hypoxic environment, the intracellular reactive oxygen species (ROS) level was measured by DCFH2-DA. The cells were washed with PBS and then incubated with 100 μL of serum-free DMEM containing 1 μM DCFH2-DA and 10 μM Hoechst for 30 min at 37 °C. After incubation, the cells were washed with PBS to remove the extra dye and then covered with 100 μL of PBS. Images were taken immediately and analyzed by a high content screening (HCS) system (Thermo, USA).

### Immunofluorescence staining of BMPR2 in hypoxia-induced HPASMCs

The expression of bone morphogenetic protein receptor 2 (BMPR2) in HPASMCs was determined by immunofluorescence staining. After treatment, cells were washed with PBS and fixed with 4% paraformaldehyde at room temperature. Then, the cells were permeabilized with 0.5% Triton X-100 and blocked with 3% BSA for 1 h at 37 °C. After that, cells were immunostained with the primary antibody for BMPR2 overnight at 4 °C, and then incubated with Alexa 555-conjugated secondary antibody (diluted 1:500) for 1 h at room temperature followed by incubation with 10 μM Hoechst 33342 for 15 min away from light. Images were taken immediately and analyzed by the HCS system.

### Western blotting

Lung tissues and right ventricles were lysed with RIPA lysis buffer (Cell Signaling Technology, USA) supplemented with a cocktail of protease inhibitors. Lysates were centrifuged at 12,000 × *g* for 20 min at 4 °C, and the supernatant was collected as total protein. A BCA protein assay kit (Cwbio, China) was used to measure the amounts of protein in each extract. Equal amounts (50 μg) of protein extracts were subjected to SDS-PAGE and electrotransferred to a polyvinylidene difluoride (PVDF) membrane. The PVDF membranes were then blocked with 5% BSA at room temperature for 1.5 h. After washing, the blots of lung homogenates were incubated with primary antibodies against BMPR2, p-Smad1/5$^{(Ser463/465)}$, Smad1/5, Bax, Bcl-2, PCNA, PPARγ, p-PI3K$^{(Tyr458)}$, PI3K, p-Akt$^{(Ser473)}$, Akt and eNOS, and blots of right ventricular homogenates were incubated with primary antibodies against PPARγ, PI3K, p-Akt$^{(Ser473)}$, Akt, p-GSK3β$^{(Ser9)}$, GSK3β, Nrf2, NOX4, and HO-1 overnight at 4 °C. After washing and incubation with HRP-conjugated secondary antibody (1:5000) (Cwbio, China) at room temperature for 1 h, the blots were exposed to a ChemiDoc-It Imaging System (UVP, USA), and the immunoreactivity bands were visualized by enhanced chemiluminescence (Cwbio, China).

### Statistical analysis

One-way analysis of variance (one-way ANOVA) or two-way analysis of variance (two-way ANOVA) was used to compare the data among different groups. $P < 0.05$ was considered statistically significant.

## RESULTS

### Puer-V alleviated the MCT-induced increase in RVSP and attenuated lung injury

PAH is generally caused by pulmonary vascular remodeling, and the increased pulmonary artery pressure caused by vascular remodeling leads to increased right ventricular afterload, which is manifested by increased RVSP. The results (Fig. 2a) showed that, at the end of the experiment on the 28th day after model establishment, the RVSP of the model rats was increased compared with that of the normal rats. Different doses of Puer-V, Puer, and the positive drug, bosentan remarkably reduced RVSP of diseased rats.

Patients with PAH often experience pathological changes such as pulmonary edema and bleeding. At the end of the experiment, the lung tissues were weighed and the lung mass index was calculated (Fig. 2b). The lung tissues were stained with H&E to

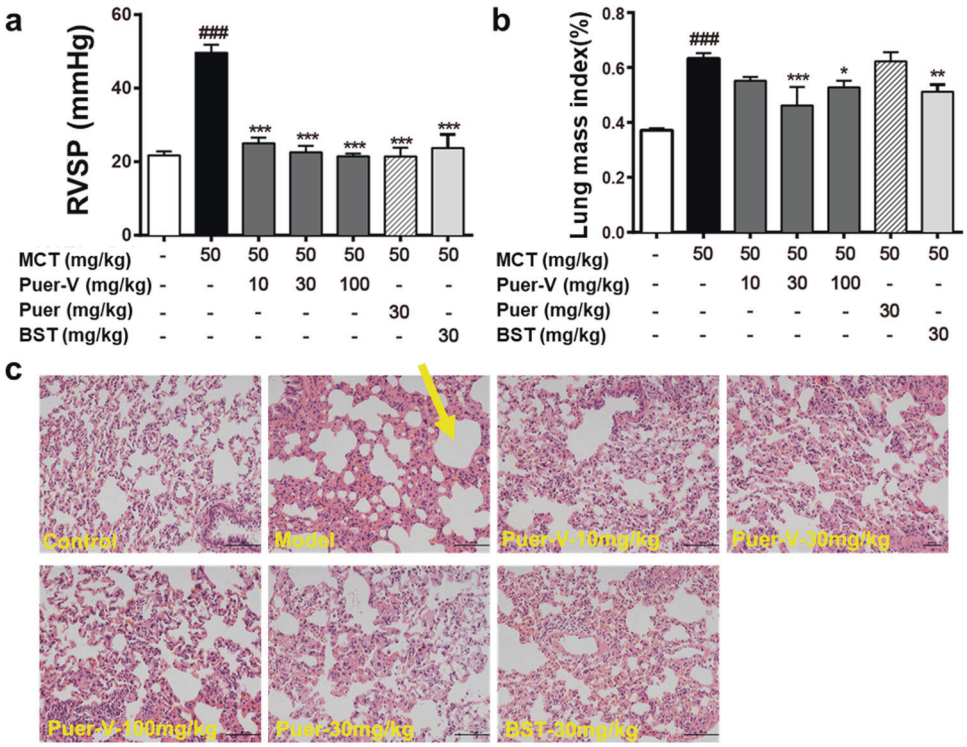


**Fig. 2 Effects of Puer-V on RVSP and lung injury in rats with MCT-induced PAH. a** RVSP of rats in different groups. **b** The weight ratio of the lung to the whole body. The results are presented as the mean ± SEM, $^{###}P < 0.001$ vs. the control group, $^{*}P < 0.05$, $^{**}P < 0.01$, $^{***}P < 0.001$ vs. the model group. $n = 15$. **c** Representative photos of lung tissues stained by H&E (×200). The yellow arrow indicates the area of edema.

observe the changes in the microstructure of rat alveoli. The model rats showed alveolar rupture and edema. Each administration group showed improvement. The therapeutic effect of Puer-V was better than that of Puer (Fig. 2c).

Puer-V improved pulmonary artery blood flow

During the process of PAH, pulmonary artery vascular resistance gradually increases and vascular hemodynamics changes. In this study, small animal echocardiography was used to detect pulmonary artery hemodynamics in rats with PAH. The PAAT, PA VIT, and $PV_{max}$ of the diseased rats were remarkably reduced compared with those of the normal rats (Fig. 3). After drug intervention, the above indicators showed a certain trend of improvement. The high dose of Puer-V showed the best effect in improving pulmonary artery blood flow, but there was no significant difference in the improvement of PA VIT and $PV_{max}$.

Puer-V improved pulmonary vasodilation and contraction function in the rats with PAH

Due to damage to the pulmonary artery endothelium, the vasodilation and contraction function of the blood vessels are impaired. The contractile response of pulmonary arteries to Phe and ET-1 was reduced in the diseased rats (Fig. 4a–d). Puerarin increased pulmonary artery reactivity in a concentration-dependent manner. The vasodilatory effect of pulmonary arteries induced by ACh and SNP was weakened in the model rats, and the administration of puerarin increased the sensitivity of pulmonary arteries. The vasodilatory activity, especially the vasodilatory effect induced by ACh, showed that puerarin had a certain protective effect on pulmonary arteries, thus maintaining the vasodilation and contraction of pulmonary arteries. EVG staining results (Fig. 4e, f) indicated that Puer-V effectively alleviated the remodeling of pulmonary arteries of different diameters, especially vessels less than 150 μm in diameter. The level of ET-1 in lung tissue homogenates was also detected. The level of ET-1 in the lung tissues of the model rats was strikingly increased (Fig. 4g). Puer-V effectively reduced ET-1 levels in lung tissues of the rats with MCT-induced PAH.

Puer-V inhibited the inflammatory response in lung tissues

At the end of the experiment, the lungs were harvested and the lung sections were immunostained for CD68. CD68 is a marker of macrophages, which reflects the severity of inflammatory response. The expression of CD68 increased in the model rats (Fig. 5a), and each administration group showed improvement. The quantitative results of inflammatory factor detection indicated that the level of IL-6 in lung tissues of the model rats was remarkably increased (Fig. 5b). Puer-V and bosentan reduced the level of IL-6 in lung tissues.

Puer-V attenuated right ventricular injury and maintained normal function of the right ventricle

In this study, we used small animal echocardiography to observe the structural and functional changes in the right ventricle of rats with PAH. The thickness of the right ventricular wall and the width of the right ventricular cavity of the diseased rats increased, indicating hypertrophy and dilatation of the right ventricle (Fig. 6a–e). After drug administration, right ventricular remodeling was attenuated to a certain extent. The right ventricular output and stroke volume of the model rats were decreased to a certain extent. Puer-V increased the stroke volume in a concentration-dependent manner, and the improvement was better than that of bosentan. Organ index measurements also indicated right ventricular hypertrophy in the rats with MCT-induced PAH. The weight ratio of the right ventricle to the whole body and right ventricular hypertrophy index was markedly increased in the model rats (Fig. 6f, g). Puerarin and bosentan reduced the weight ratio of the right ventricle. Puer-V showed a better effect than bosentan and Puer.

NT-pro BNP is an auxiliary diagnostic marker of heart failure and cTnT is a marker of myocardial infarction, both of which are widely

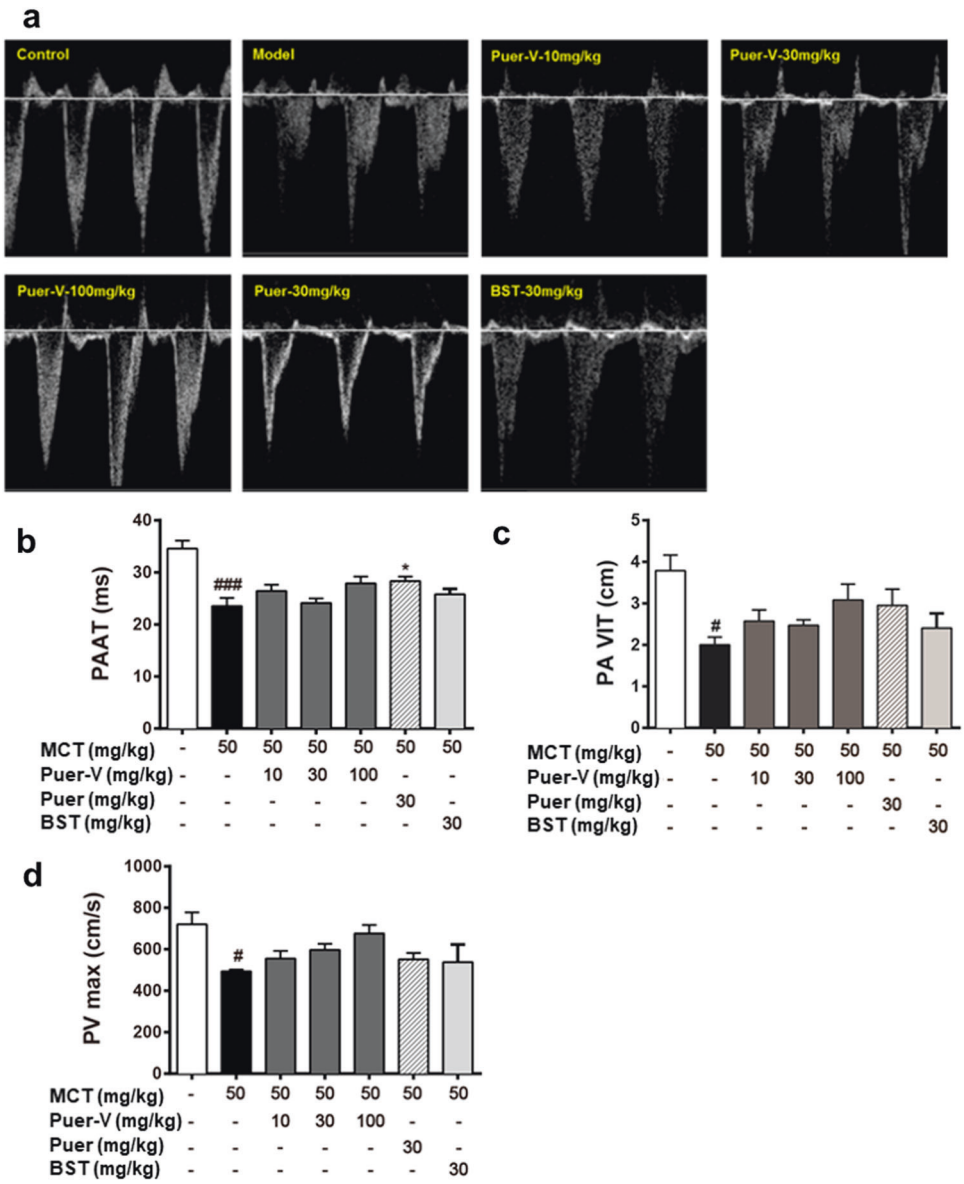


**Fig. 3 The influence of Puer-V on the pulmonary artery blood flow of the rats with PAH. a** Representative pictures of pulmonary blood flow. **b** PAAT, **c** PA VIT, and **d** $PV_{max}$ of the rats in each group. The results are presented as the mean ± SEM, $^{\#}P < 0.05$, $^{\#\#\#}P < 0.001$ vs. the control group, $^{*}P < 0.05$ vs. the model group, $n = 3$.

used in the evaluation of the degree of myocardial damage [12]. In this experiment, the levels of NT-pro BNP and cTnT in the serum were measured to evaluate the degree of myocardial damage in the rats with MCT-induced PAH. The contents of NT-pro BNP and cTnT in the serum of the model rats increased (Fig. 6h, i). There was a certain downward trend after administration of different doses of Puer-V and bosentan, but the difference was not statistically significant. The high dose of Puer-V had the best efficacy in attenuating myocardial damage in the rats with MCT-induced PAH.

In the process of PH, right ventricular dysfunction is often accompanied by cardiac ischemia, which is manifested as a decrease in microvessel density in the right myocardium [13]. In the present study, CD31 immunostaining was performed on right ventricular wall slices, and the density of blood vessels was calculated. The expression level of CD31 in the right ventricle of the model rats decreased. After drug intervention, Puer-V increased the expression of CD31 in a concentration-dependent manner (Fig. 6j, k). The results indicated that Puer-V effectively restored the normal function of the right ventricle in the rats with MCT-induced PAH.

### Puer-V improved right ventricular remodeling in the rats with MCT-induced PAH through PPARγ/PI3K/Akt and oxidative stress pathways

Morphological changes in cardiomyocytes in the right ventricular wall were observed by H&E staining, and collagen deposition in the right ventricle was observed by Masson staining. Myocardial hypertrophy, swelling, and lengthening were observed in the model rats (Fig. 7a, c), with unclear myocardial fibers and collagen deposition (Fig. 7b, d). Puer-V and bosentan not only reduced the size of myocardial cells, but also improved myocardial remodeling and ameliorated collagen deposition. Puer-V showed a better effect than bosentan in maintaining the normal structure of the right ventricle of the rats with MCT-induced PAH.

To study the underlying mechanism of Puer-V-mediated improvement in the right ventricle, we used an immunoblotting assay. In recent years, experimental studies have found that

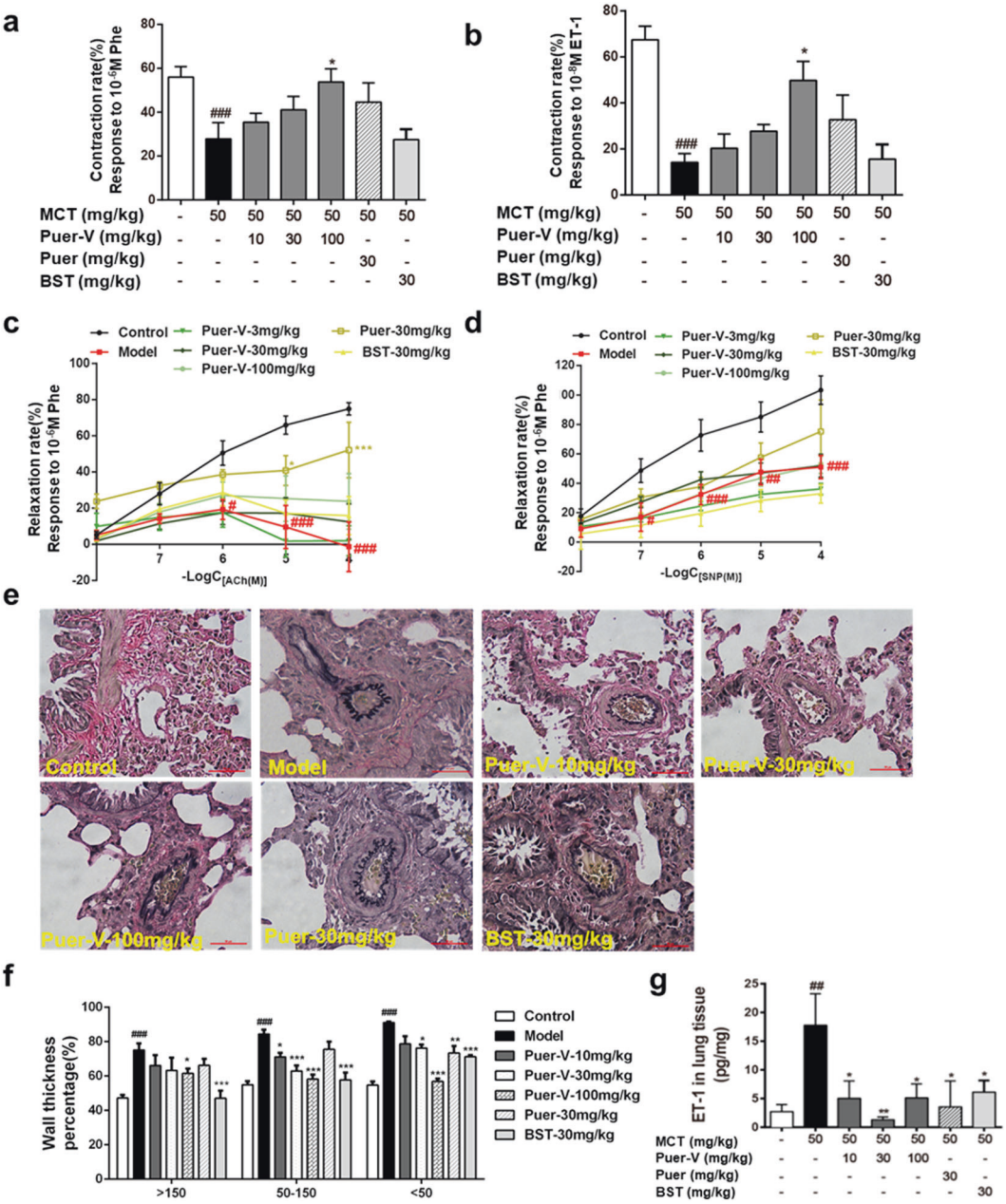


**Fig. 4 The influence of Puer-V on pulmonary vascular compliance.** **a** Contraction rate response to 1 μM Phe, **b** contraction rate response to 0.01 μM ET-1, **c** relaxation induced by ACh in pulmonary arteries preconstricted by 1 μM Phe, **d** relaxation induced by SNP in pulmonary arteries preconstricted by 1 μM Phe. **e** EVG staining of pulmonary arteries (400×) and **f** quantitative results of the wall thickness percentage. **g** The level of ET-1 in lung tissues of the rats with PAH. The results are presented as the mean ± SEM, $^{\#}P < 0.05$, $^{\#\#}P < 0.01$, $^{\#\#\#}P < 0.001$ vs. the control group, $^{*}P < 0.05$, $^{**}P < 0.01$, $^{***}P < 0.001$ vs. the model group. $n = 6$.

peroxisome proliferator-activated receptor-γ (PPARγ) activation could inhibit oxidative stress [14] and had a certain protective effect on the myocardium [15]. The PI3K/Akt pathway reduces the apoptosis and hypertrophy of cardiomyocytes by regulating the phosphorylation of downstream GSK3β [16]. In the present study, the expression levels of PPARγ, PI3K, Akt, and GSK3β in the right ventricle of the model rats were downregulated (Fig. 7e–h), and Puer-V improved this phenomenon and showed better effects than bosentan.

Oxidative stress refers to the imbalance between oxidation and antioxidation, and the increase in oxidative substances directly damages tissues and organs. Right ventricular hypertrophy caused by pulmonary hypertension is closely related to oxidative stress. NOX4 is an important member of the NADPH oxidase family, which can promote the generation and release of ROS [17] and induce immune and inflammatory response [18]. Nrf2 (NF-E2-related factor2) is a key regulator of the cellular oxidative stress response. It exerts anti-inflammatory and oxidative stress roles by regulating downstream heme oxygenase 1 (HO-1) [19]. The heme degradation products catalyzed by HO-1 can resist oxidative damage, protect myocardial cells and inhibit myocardial apoptosis [20]. In the present experiment, the NOX4 level was increased and the Nrf2 and HO-1 levels were decreased in the right ventricle of the rats with MCT-induced PAH (Fig. 7i–k). After Puer-V administration, this phenomenon was improved. The results indicated that Puer-V effectively inhibited the oxidative stress response in the right ventricle of the rats with MCT-induced PAH, which could be the potential mechanism for improving right ventricular remodeling.

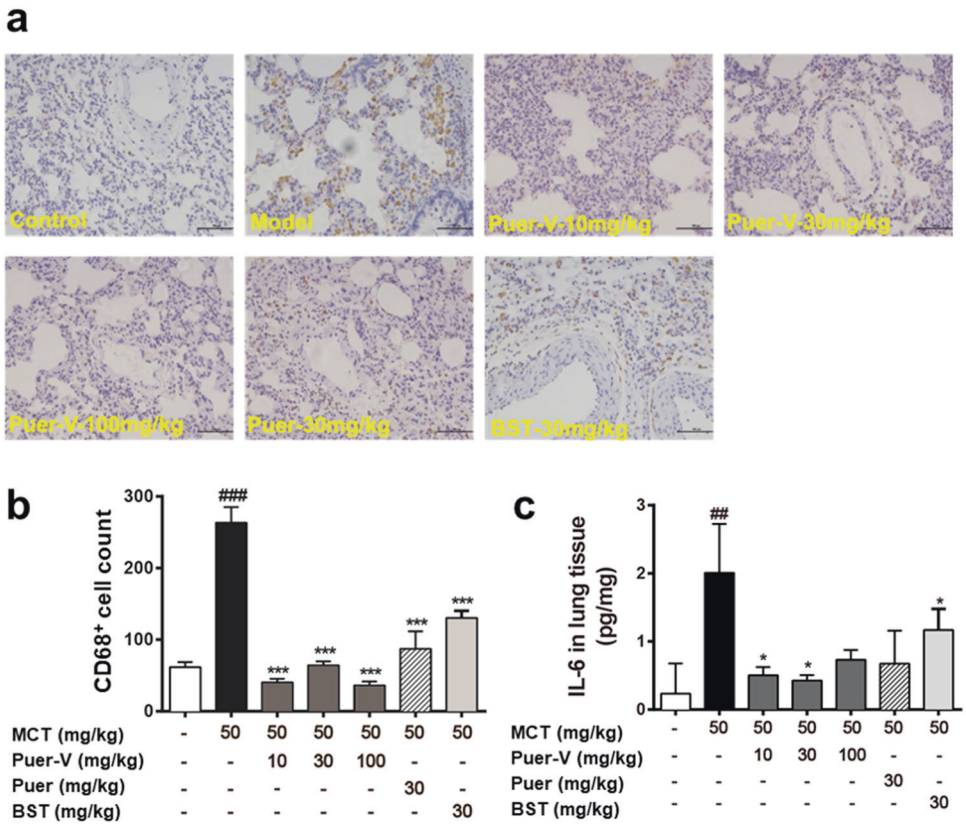


**Fig. 5 The influence of Puer-V on the inflammatory response in lung tissues.** Immunohistochemistry for CD68 on lung sections. The photos were obtained from an optical microscope (**a**) (200×), and quantification of CD68 positive cells was performed by ImageJ (**b**). The influence of Puer-V on IL-6 (**c**) in lung tissues of the rats with PAH. The results are presented as the mean ± SEM, $^{\#\#}P < 0.01$, $^{\#\#\#}P < 0.001$ vs. the control group, $^{*}P < 0.05$, $^{***}P < 0.001$ vs the model group, $n = 6$.

Puer-V showed therapeutic effects on mice with HPH

The therapeutic effect of Puer-V on HPH was assessed in a two-week hypoxia mouse model. The results (Fig. 8b) showed that the murine HPH model was successfully established, as the RVSP of the mice with HPH was strikingly increased. Preadministration of Puer-V attenuated the weight loss (Fig. 8a) and the elevation in RVSP induced by hypoxia. Due to cardiopulmonary dysfunction, the diseased mice showed a weak athletic ability. The running distance of the mice on a treadmill at accelerating speed until exhaustion was decreased (Fig. 8c). Puer-V and Puer could effectively improve the walking distance of the mice with HPH. In this two-week hypoxia mouse model, the right ventricular hypertrophy index was not significantly increased (Fig. 8d). Puer-V improved the lung index (Fig. 8e) and spleen index (Fig. 8f) in the mice with HPH. In brief, Puer-V exhibited a more potent effect on hemodynamic indicators and exercise performance than sildenafil.

Puer-V inhibited the downregulation of BMPR2/Smad signaling pathway in the rats with MCT-induced PAH and mice with hypoxia-induced HPH

BMPR2 belongs to the TGFβ superfamily. Its activation inhibits smooth muscle cell proliferation and induces apoptosis by regulating the expression of Bcl-2 and other related proteins. BMPR2 is an activator of the type I receptor, which activates downstream Smads, and induces their nuclear translocation to regulate the transcription process of genes. Mutation of BMPR2 gene causes transcriptional termination, leading to excessive cell proliferation and apoptosis inhibition. The expression of BMPR2 and phosphorylated Smad1/5 was downregulated in the model group (Fig. 9), and upregulated after the administration of the positive control drugs and Puer-V. The results indicated that puerarin can help maintain the expression of BMPR2 and p-Smad1/5.

The influence of Puer-V on the PPARγ/PI3K/Akt signaling pathway in lung tissues of the rats with MCT-induced PAH and mice with hypoxia-induced HPH

PPARγ is a downstream effector of BMPR2 and the PPARγ/PI3K/Akt signaling pathway also plays an important role in the pathological changes of the pulmonary artery in animals and patients with PH [21–23]. PPARγ activation can improve the muscularization and vascular remodeling of pulmonary arterioles [24], reduce the expression of vasoconstrictive substances such as ET-1 [25], and improve vascular function [26]. PI3K/Akt promotes the production of NO by regulating the expression of downstream eNOS protein, and then dilates blood vessels [27]. The expression levels of PPARγ, PI3K, P-Akt/Akt, and eNOS in the model group were all downregulated. Puer-V and positive control drugs effectively restored the expression of these proteins (Fig. 10). This finding indicated that Puer-V might promote the production of NO in pulmonary blood vessels to exert vasodilatory effects and improve vascular remodeling by regulating the PPARγ/PI3K/Akt signaling pathway.

Puer-V improved resistance to apoptosis and abnormal proliferation in lung tissues of the rats with MCT-induced PAH and mice with hypoxia-induced HPH

The pulmonary blood vessels of patients with pulmonary hypertension are often accompanied by abnormal proliferation and migration of smooth muscle cells, leading to occlusion in blood vessels and limited blood flow. In this experiment, proliferation- and apoptosis-related proteins in lung tissue were

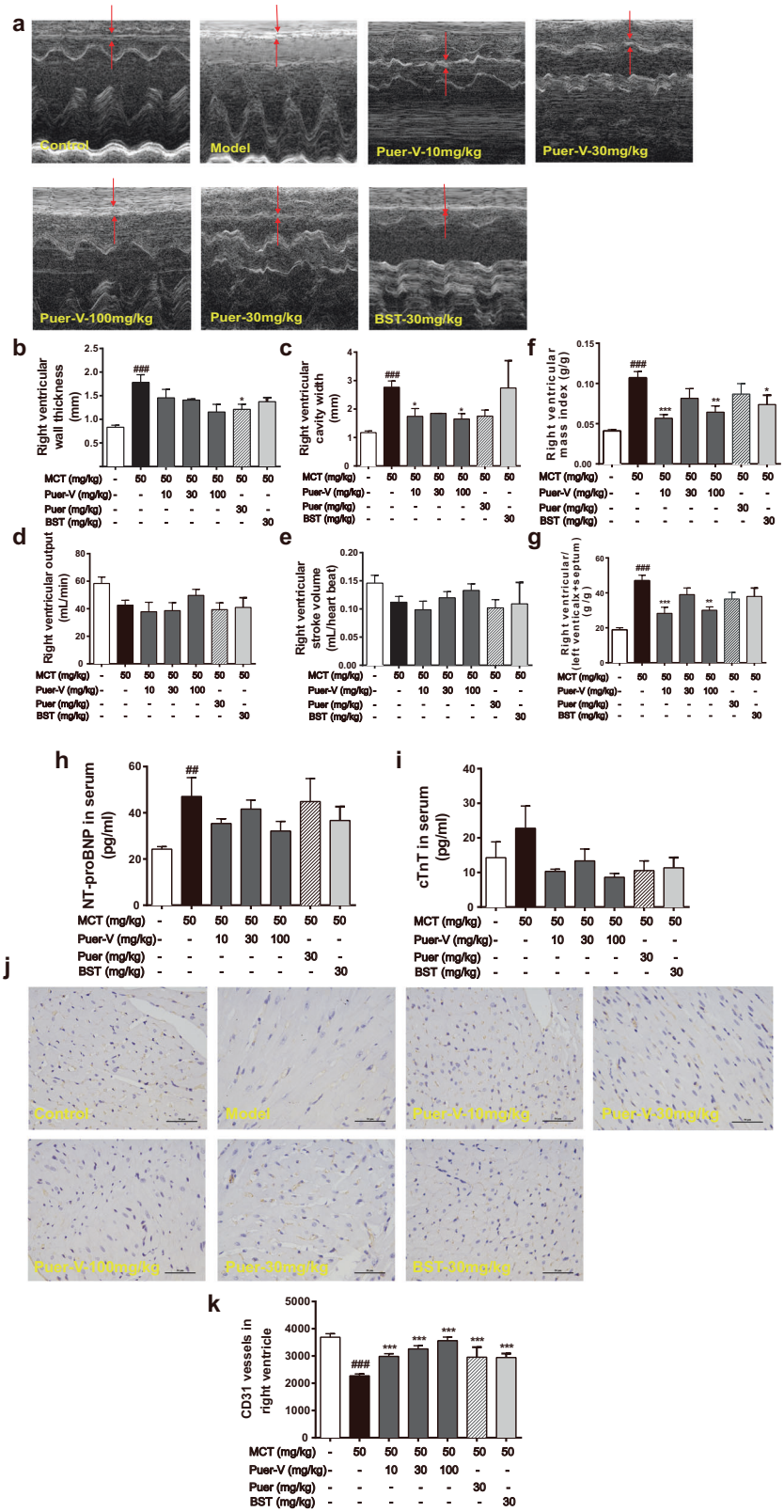


**Fig. 6 Effects of Puer-V on right ventricular function and myocardial damage in the rats with MCT-induced PAH. a** Representative images of M-mode recording through the right ventricle. **b** Right ventricle wall thickness, **c** right ventricle cavity width, **d** right ventricular output and **e** right ventricular stroke volume of rats in each group. The weight ratio of **f** the right ventricle to the whole body and **g** the right ventricular hypertrophy index of rats in each group. Detection of NT-pro BNP (**h**) and cTnT (**i**) levels in serum ($n = 6$). The influence of Puer-V on the microvessel density of the right ventricle was detected by CD31 staining, and photos (**j**) were obtained from optical microscope (×400) and analyzed by ImageJ (**k**). The results are presented as the mean ± SEM, $^{\#\#}P < 0.01$, $^{\#\#\#}P < 0.001$ vs. the control group, $^{*}P < 0.05$, $^{**}P < 0.01$, $^{***}P < 0.001$ vs. the model group, $n = 4$.

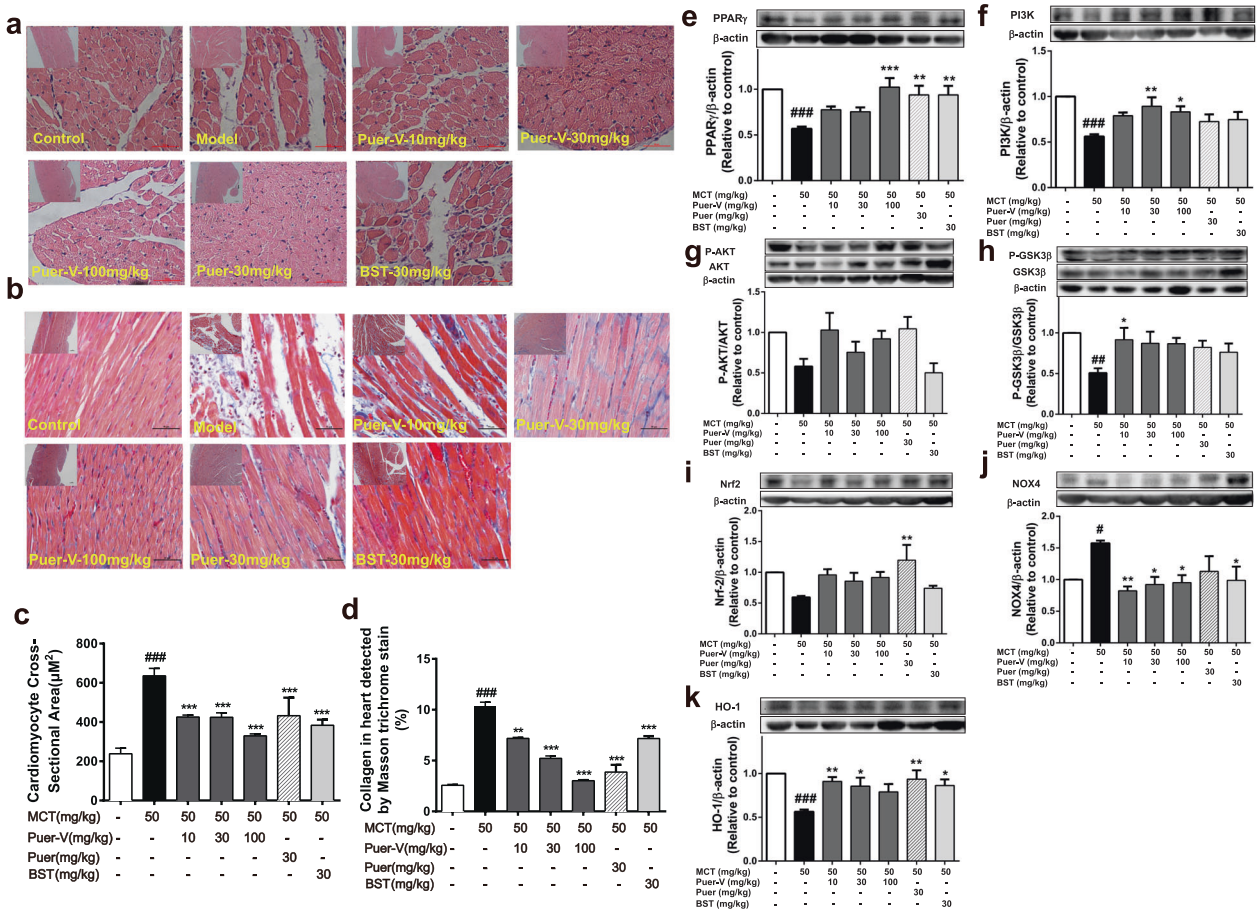


**Fig. 7 Effects of Puer-V on right ventricular remodeling.** The shape of right ventricular cardiomyocytes was detected by H&E staining, and photos were obtained with an optical microscope (**a**) and analyzed by ImageJ (**c**). The influence of Puer-V on collagen deposition in the right ventricle was detected by Masson staining. Photos were obtained with an optical microscope (**b**) and analyzed by ImageJ (**d**). (Small images magnified ×100; large images magnified ×400). **e**–**k** The influence of Puer-V on PPARγ/PI3K/Akt pathway and oxidative pathway in the right ventricle of the rats with MCT-induced PAH. Densitometric analysis of the relative expression level of each protein compared to β-actin is shown in the lower panel, and representative pictures are shown in the upper panel. The results are presented as the mean ± SEM, $^{\#}P < 0.05$, $^{\#\#}P < 0.01$, $^{\#\#\#}P < 0.001$ vs. the control group, $^{*}P < 0.05$, $^{**}P < 0.01$, $^{***}P < 0.001$ vs. the model group, $n = 4$.

detected (Fig. 11). The expression ratio of Bax/Bcl-2 in the model group was downregulated, and there was a certain increasing trend after drug administration but no significant difference. The expression level of PCNA was upregulated in the diseased animals, and after drug intervention the expression level was downregulated in a concentration-dependent manner, indicating that Puer-V inhibited the abnormal proliferation of cells in the smooth muscle layer.

Puer-V inhibited the proliferation of hypoxia-induced HPASMCs
No cytotoxicity in HPASMCs was induced by Puer-V at concentrations up to 100 μM (Fig. 12a), indicating that relevant pharmacodynamic studies were allowed to be carried out in this concentration range. The inhibitory effect of Puer-V on proliferation was carried out on HPASMCs induced by hypoxia for 48 h. The results (Fig. 12b) showed that the viability of HPASMCs was elevated after incubation for 48 h under hypoxic conditions. Puer-V inhibited the proliferation of HPASMCs induced by hypoxia, and 3 μM Puer-V showed the best inhibitory effect.

Puer-V decreased ROS formation in hypoxia-induced HPASMCs
A DCFH fluorescent probe was used to detect cytoplasmic ROS in HPASMCs, which could enter the cell and be enzymatically cleaved to be oxidized by ROS to generate fluorescent DCF. Hypoxia treatment strikingly increased ROS levels compared with those of HPASMCs under normoxic conditions (Fig. 13). Different doses of Puer-V alleviated this phenomenon to some extent, thereby alleviating the oxidative stress response in HPASMCs induced by hypoxia.

Puer-V restored BMPR2 expression in hypoxia-induced HPASMCs
Downregulation of BMPR2 expression in HPASMCs will cause excessive cell proliferation with apoptosic resistance. In the present study, the results indicated the loss of BMPR2 expression in hypoxia-induced HPASMCs. Puer-V (3 μM and 30 μM) could upregulate BMPR2 levels to some extent (Fig. 14). This finding indicated that Puer-V exerted protective effects on hypoxia-induced HPASMCs by restoring the expression of BMPR2.

## DISCUSSION

Although major advances have been made in the treatment of PH in the past forty years, commercially available drugs still cannot meet the current clinical needs, and the mortality of PH patients is still high. Because PH is a progressive disease, currently existing drugs mainly alleviate symptoms but show unsatisfactory effects on the critical pathological changes of PH, such as vascular and right ventricular remodeling [28]. In recent years, a growing body of research has shown that the BMPR2 and PPARγ signaling pathways play an important role in the pathological process of PH.

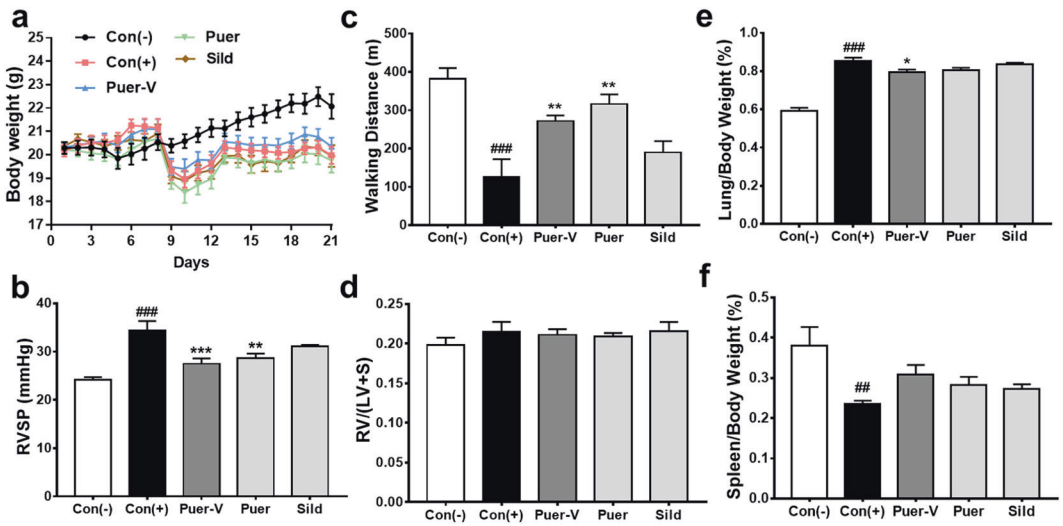


**Fig. 8 Efficacy of Puer-V on the mice with HPH. a** Body weight change of mice in different groups during the experiment. The influence of Puer-V on **b** RVSP, **c** walking distance, **d** right ventricular hypertrophy index, **e** lung index and **f** spleen index. The results are presented as the mean ± SEM, $^{\#\#}P < 0.01$, $^{\#\#\#}P < 0.001$ vs. the control group, $^{*}P < 0.05$, $^{**}P < 0.01$, $^{***}P < 0.001$ vs. the model group, $n = 6$.

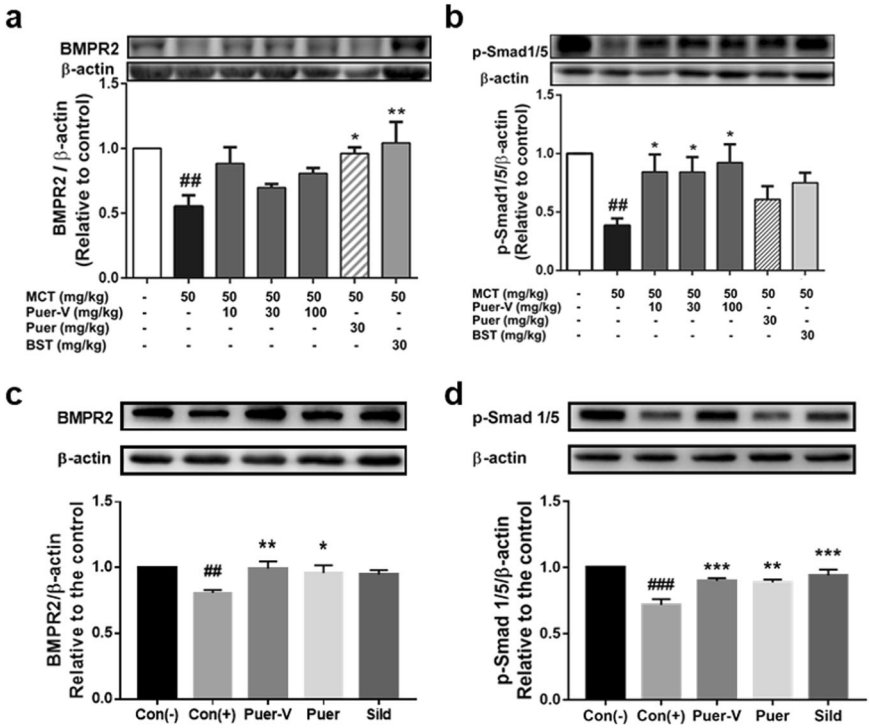


**Fig. 9 Effects of Puer-V on the BMPR2/Smad pathway in lung tissues of the rats with PAH and mice with HPH.** Densitometric analysis of the relative expression level of each protein compared to β-actin is shown in the lower panel, and representative pictures are shown in the upper panel: **a** BMPR2 and **b** p-Smad1/5 in lung tissues of the rats with PAH, **c** BMPR2 and **d** p-Smad1/5 in lung tissues of mice with HPH. The results are presented as the mean ± SEM, $^{\#\#}P < 0.01$, $^{\#\#\#}P < 0.001$ vs. the control group, $^{*}P < 0.05$, $^{**}P < 0.01$, $^{***}P < 0.001$ vs. the model group, $n = 4$.

Studies have shown that the PPARγ signaling pathway can even reverse the pathological process of PH [29]. Thus, in this study, we intended to explore whether the therapeutic effect of Puer-V is related to these two pivotal signaling pathways. Based on our study, we hope to provide more evidence for the clinical use of puerarin for PH.

Years of research have led to a variety of animal models for preclinical study of PH. In the present study, two types of animal models of PH were successfully established and used for the mechanistic study (Figs. 2a and 8b). The mechanism by which MCT causes rat PAH involves liver metabolites of MCT damaging the pulmonary arterial endothelium. Endothelial dysfunction will cause the abnormal proliferation of pulmonary arterial smooth cells and excessive apoptosis of pulmonary arterial endothelial cells [30, 31]. The remodeled pulmonary vasculature will then cause elevation in pulmonary arterial pressure and RVSP. Hypoxia induces HPH in mice because oxygen deficiency in the pulmonary circulation causes endothelial damage and abnormal contraction

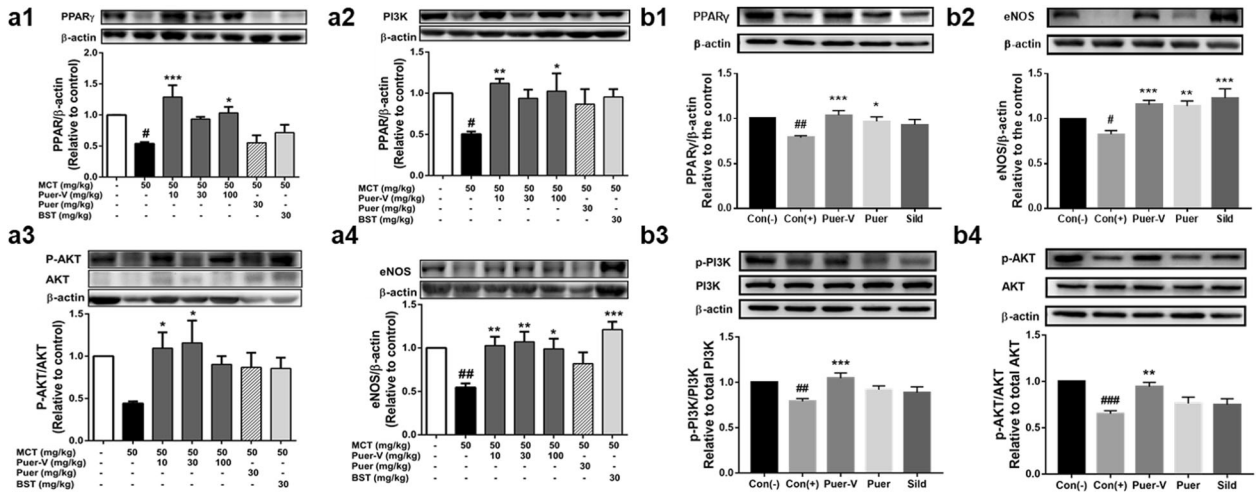


**Fig. 10 Effects of Puer-V on the PPARγ/PI3K/Akt pathway in lung tissues of the rats with PAH and mice with HPH.** Densitometric analysis of the relative expression level of each protein compared to β-actin is shown in the lower panel, and representative pictures are shown in the upper panel: **a1** PPARγ, **a2** PI3K, **a3** p-Akt/Akt, and **a4** eNOS in lung tissues of the rats with PAH. **b1** PPARγ, **b2** eNOS, **b3** p-PI3K/PI3K, and **b4** p-Akt/Akt in lung tissues of mice with HPH. The results are presented as the mean ± SEM. $^{\#}P < 0.05$, $^{\#\#}P < 0.01$ vs. the control group, $^{*}P < 0.05$, $^{**}P < 0.01$, $^{***}P < 0.001$ vs. the model group, $n = 4$.

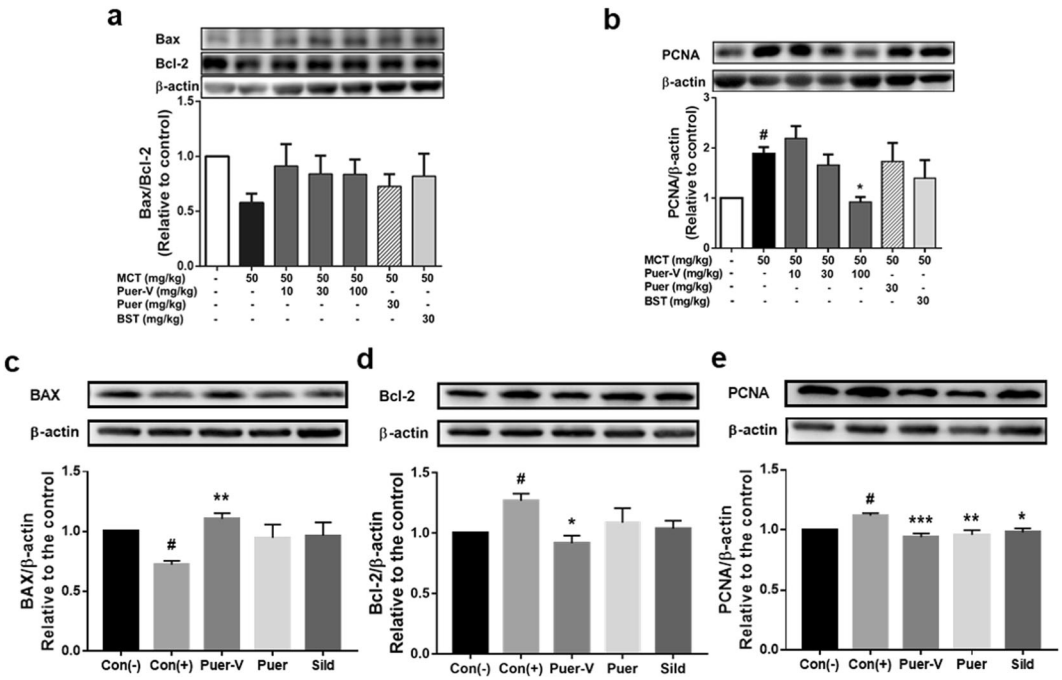


**Fig. 11 Effects of Puer-V on apoptosis and proliferation in lung tissues of the rats with PAH and mice with HPH.** Densitometric analysis of the relative expression level of each protein compared to β-actin is shown in the lower panel, and representative pictures are shown in the upper panel: **a** Bax, Bcl-2 and **b** PCNA in lung tissues of the rats with PAH. **c** Bax, **d** Bcl-2, and **e** PCNA in lung tissues of mice with HPH. The results are presented as the mean ± SEM, $^{\#}P < 0.05$ vs. the control group, $^{*}P < 0.05$, $^{**}P < 0.01$, $^{***}P < 0.001$ vs. the model group, $n = 4$.

of the pulmonary artery [32]. Both animal models can effectively simulate the pathological process of clinical PH patients [33]. In the present study, puerarin was used to intervene in the early stage of the disease process to explore the preventive effect of puerarin on PH.

BMPR2, a member of the TGFβ receptor superfamily, plays a critical role in the etiology of PAH. BMP signaling plays a key role in vascular homeostasis by inhibiting abnormal vascular remodeling [34], as BMPR2 is a negative regulator of smooth muscle cells and a survival factor of endothelial cells [35]. PPARγ is abundantly expressed in normal lungs, with the highest levels in the lungs compared with other organs [36]. In the lungs of patients with PH, the expression of PPARγ is decreased [37]. Extensive evidence indicates that PPARγ, a downstream effector of BMPR2, is involved in the regulation of cellular differentiation, development, metabolism, inflammation, and tumorigenesis and favorably affects several pathways associated with the pathogenesis of PH [34, 38]. PPARγ can promote PI3K expression, which further activates Akt and phosphorylates eNOS to produce NO [39]. Our previous study indicated that puerarin exerted protective effects on pulmonary artery endothelial cells from hypoxia-induced injury through the BMPR2 and PPARγ signaling pathways [23]. In the present study, we found that the BMPR2/Smad1/5 and PPARγ/PI3K/Akt/eNOS pathways were notably altered in PAH and HPH animal models

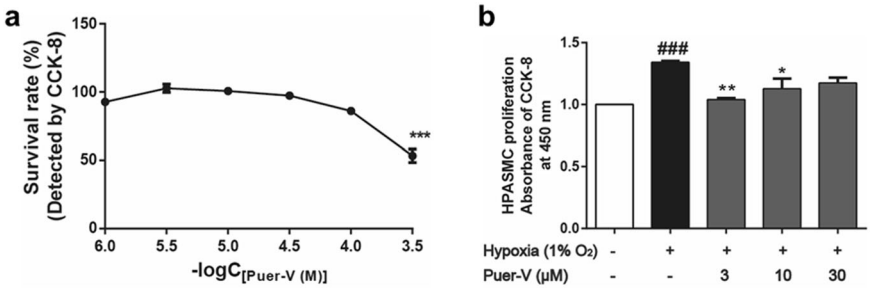


**Fig. 12 Effects of Puer-V on the proliferation of HPASMCs induced by hypoxia. a** The cytotoxicity of Puer-V on HPASMCs. **b** The effect of Puer-V on the proliferation of HPASMCs induced by hypoxia (1% $O_2$). Values are expressed as the mean ± SEM, $^{***}P < 0.001$ vs. the vehicle group for figure **a**. $^{###}P < 0.001$ vs. the normoxia group, $^{*}P < 0.05$, $^{**}P < 0.01$ vs. the hypoxia group for figure **b**, $n = 6$.

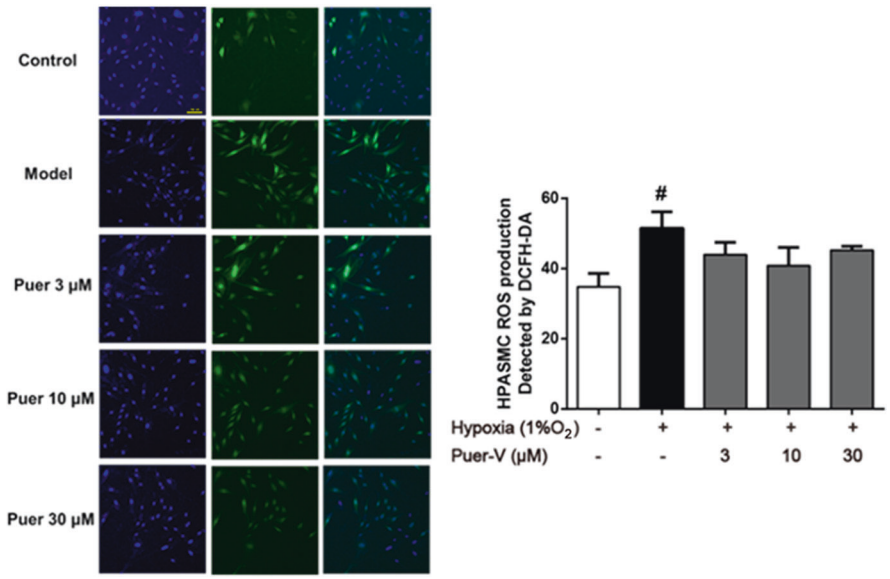


**Fig. 13 Effects of Puer-V on ROS formation in HPASMCs induced by hypoxia.** Representative images (magnified ×200) produced by the HCS system are shown in the left panel. Quantitative results of fluorescence intensity are shown in the right panel. Values are expressed as the mean ± SEM. $^{#}P < 0.05$ vs. the control group. $n = 3$.

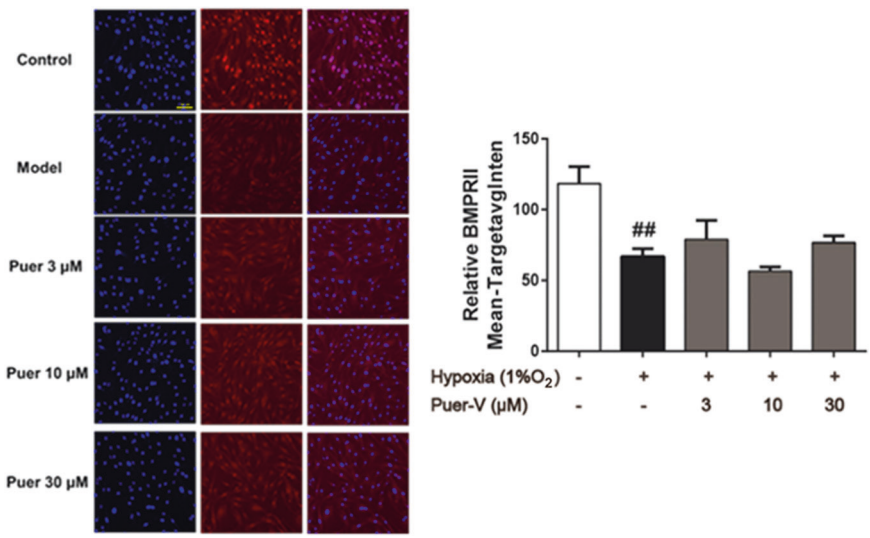


**Fig. 14 Effects of Puer-V on BMPR2 expression in HPASMCs induced by hypoxia.** Representative images (magnified ×200) produced by the HCS system are shown in the left panel. Quantitative results of fluorescence intensity are shown in the right panel. Values are expressed as the mean ± SEM, $n = 3$. $^{##}P < 0.01$ vs. the control group. $n = 3$.

(Figs. 9 and 10). Puer-V effectively improved this phenomenon and showed a good therapeutic effect on PH.

The pathological processes of PAH and HPH are both initiated in the pulmonary artery, after which pulmonary arterial smooth muscle cells and endothelial cells undergo different pathological processes. These changes trigger the abnormal proliferation and contraction of smooth muscle cells and endothelial dysfunction [40]. In our study, the rat model of MCT-induced PAH showed significant dysfunction in pulmonary arteries. Echocardiography results showed obstruction in pulmonary arteries. EVG staining indicated obvious pulmonary arterial remodeling (Fig. 4e, f). The in vitro vascular function experiment also indicated vascular systolic and diastolic dysfunction of the main pulmonary artery (Fig. 4a–d). Puer-V could effectively improve the abnormal changes in structure and function in pulmonary arteries (Figs. 3 and 4). In addition, the endothelial injury could trigger the secretion of ET-1, which would cause the abnormal contraction of smooth muscle cells [41]. In our study, we found that Puer-V could reduce ET-1 levels in lung tissues (Fig. 4g). This finding could also explain the above improvement effect of Puer-V on the pulmonary arteries.

A series of pathological changes in the cells of lung tissues could cause pulmonary injury, edema, and inflammation [42], which was indicated by the increased lung index and the morphology of lung tissue sections stained by H&E (Fig. 2c). CD68 staining and IL-6 level detection also indicated a severe inflammatory response in lung tissues (Fig. 5). Due to the impairment of lung function, the exercise capacity of the diseased animals remarkably declined. Puer-V attenuated pulmonary edema and inflammatory factor accumulation in the diseased animals. A mechanism study indicated that Puer-V could restore the expression of BMPR2 and PPARγ in lung tissues, thus maintaining the protective effect of the BMPR2/Smad pathway and PPARγ/PI3K/Akt/eNOS pathway on lung tissues. In addition, markers related to proliferation and apoptosis, including PCNA, Bax, and Bcl-2, were detected. The results indicated that Puer-V could attenuate apoptotic resistance and abnormal proliferation of the cells in the smooth muscle layer (Fig. 11). Therefore, Puer-V improved the exercise capability of the diseased animals by improving lung function.

Elevation in pulmonary vascular resistance then would increase right ventricular afterload and subsequent right ventricular remodeling, manifested as elevated RVSP, enlargement of ventricular chamber, and a series of pathological changes in the right ventricle [43]. Right ventricular remodeling is often accompanied by myocardial collagen deposition, reduction in myocardial vascular density and elevation in myocardial injury markers in serum [44]. H&E staining and Masson staining showed the morphological structure and arrangement of right ventricular cardiomyocytes. Compared with that of the control group, the myocardial cell volume of the model group increased, the arrangement was disordered, and collagen deposition was serious in the diseased animals (Fig. 7a–d). CD31 is a specific marker for endothelial cells that can show myocardial vascular density in the right ventricle [45]. The expression of CD31 in the right ventricle of the diseased animals was strikingly decreased (Fig. 6j, k), indicating that myocardial ischemia occurred in the right ventricle. This phenomenon is another dominant cause of the impairment of right ventricular ejection function. It is precisely due to the structural damage of the right heart that the myocardial damage markers, NT-proBNP and cTnT, in the plasma are elevated (Fig. 6h, i). Echocardiography results showed that cardiac output and ejection fraction of the right ventricle were decreased (Fig. 6a–e). Puer-V improved the impairment phenomenon, thereby improving the structure and function of the right ventricle. A molecular study indicated that the therapeutic effect of Puer-V on the right ventricle is related to the PPARγ/PI3K/Akt and oxidative stress pathways (Fig. 7e–k). Considerable clinical trials show that right ventricular failure is the primary cause of death in PH patients, and current marketed drugs have little effect on this process [46]. The therapeutic effect of Puer-V on right ventricular remodeling would provide a solid foundation for the drug development and clinical application of Puer-V for the treatment of PH.

HPASMCs are the major component of the media of pulmonary arteries [47]. Because of the abnormal contraction and proliferation of these cells upon pathological stimulation in the pathological process of PH, it is important to investigate the protective effect of Puer-V on HPASMCs. A hypoxia-induced HPASMC model was applied to provide insights into the mechanistic study. Under hypoxic conditions, the HPASMCs are activated to proliferate (Fig. 12), which is mainly caused by the reduced expression of BMPR2 [48, 49] and the accumulation of ROS in the cytoplasm [50, 51]. Puer-V intervention restored the expression of BMPR2 (Fig. 14) and inhibited the ROS level (Fig. 13) in HPASMCs. Consequently, Puer-V inhibited the abnormal proliferation of HPASMCs.

It is worth mentioning that Zhang et al. [52] reported for the first time that puerarin exerted therapeutic effects on a three-week-HPH rat model by inhibiting autophagy. Studies have reported that autophagic activation contributes to BMPR2 degradation, but whether the function is direct or through several pathways needs further investigation [53]. Notably, puerarin restored the expression of BMPR2. Their research does provide a reference for more in-depth mechanistic study of puerarin against PH.

In summary, Puer-V prevents the progression of MCT-induced four-week rat PAH and a hypoxia-induced two-week mouse model of HPH through BMPR2/Smad and PPARγ/PI3K/Akt signaling pathways. Puer-V effectively improved pulmonary arterial and right ventricular remodeling in a four-week rat PAH model, whereas the pathological changes associated with remodeling were not obvious in the two-week HPH mouse model. However, preliminary mechanistic study also showed the therapeutic effect of Puer-V on abnormal changes in the BMPR2/Smad and PPARγ/PI3K/Akt signaling pathways in a two-week HPH mouse model. This is the limitation of the present study. Based on the present study, the correlation between the BMPR2 and PPARγ signaling pathway and pathological remodeling changes in a chronic HPH animal model needs further investigation.

In conclusion, Puer-V showed a better therapeutic effect than bosentan on the abnormal structural changes and dysfunction of lung tissues and right ventricles of diseased animals through the BMPR2-PPARγ axis. Most importantly, Puer-V intervention also reversed the remodeling of the pulmonary artery and right ventricle in rats with PAH. Puer-V is promising as a new option for PH patients.

## ACKNOWLEDGEMENTS

This study was supported by the National Natural Science Foundation of China (82073853, 81773935) and CAMS Innovation Fund for Medical Sciences (2021-I2M-1-005).

## AUTHOR CONTRIBUTIONS

TYY, SBW, LHF, and GHD conceived and designed the study. YL provided Puer-V. DC, HFZ, and TYY carried out the experiments. SCS and RRW participated in the animal experiments. DC drafted the manuscript. TYY and LHF revised the manuscript.

## ADDITIONAL INFORMATION

**Competing interests:** The authors declare no competing interests.

## REFERENCES

1. Rosenkranz S, Howard LS, Gomberg-Maitland M, Hoeper MM. Systemic consequences of pulmonary hypertension and right-sided heart failure. Circulation. 2020;141:678–93.

2. Simonneau G, Montani D, Celermajer DS, Denton CP, Gatzoulis MA, Krowka M, et al. Haemodynamic definitions and updated clinical classification of pulmonary hypertension. Eur Respir J. 2019;53:1801913.
3. Poch D, Mandel J. Pulmonary hypertension. Ann Intern Med. 2021;174: ITC49–ITC64.
4. Lau EMT, Giannoulatou E, Celermajer DS, Humbert M. Epidemiology and treatment of pulmonary arterial hypertension. Nat Rev Cardiol. 2017;14:603–14.
5. Vazquez-Garza E, Bernal-Ramirez J, Jerjes-Sanchez C, Lozano O, Acuna-Morin E, Vanoye-Tamez M, et al. Resveratrol prevents right ventricle remodeling and dysfunction in monocrotaline-induced pulmonary arterial hypertension with a limited improvement in the lung vasculature. Oxid Med Cell Longev. 2020;2020:1841527.
6. Fan Y, Gu X, Zhang J, Sinn K, Klepetko W, Wu N, et al. TWIST1 drives smooth muscle cell proliferation in pulmonary hypertension via loss of GATA-6 and BMPR2. Am J Respir Crit Care Med. 2020;202:1283–96.
7. Liu M, Liu Q, Pei Y, Gong M, Cui X, Pan J, et al. Aqp-1 Gene knockout attenuates hypoxic pulmonary hypertension of mice. Arterioscler Thromb Vasc Biol. 2019;39:48–62.
8. Li X, Yuan T, Chen D, Chen Y, Sun S, Wang D, et al. Cardioprotective effects of puerarin-V on isoproterenol-induced myocardial infarction mice is associated with regulation of PPAR-γ/NF-kappaB pathway. Molecules. 2018;23:3322.
9. Zhou T, Wang Z, Guo M, Zhang K, Geng L, Mao A, et al. Puerarin induces mouse mesenteric vasodilation and ameliorates hypertension involving endothelial TRPV4 channels. Food Funct. 2020;11:10137–48.
10. Chen YC, Yuan TY, Zhang HF, Wang DS, Yan Y, Niu ZR, et al. Salvianolic acid A attenuates vascular remodeling in a pulmonary arterial hypertension rat model. Acta Pharmacol Sin. 2016;37:772–82.
11. Christou H, Hudalla H, Michael Z, Filatava EJ, Li J, Zhu M, et al. Impaired pulmonary arterial vasoconstriction and Nitric Oxide–mediated relaxation underlie severe pulmonary hypertension in the Sugen-hypoxia rat model. J Pharmacol Exp Ther. 2018;364:258–74.
12. Filusch A, Giannitsis E, Katus HA, Meyer FJ. High-sensitive troponin T: a novel biomarker for prognosis and disease severity in patients with pulmonary arterial hypertension. Clin Sci. 2010;119:207–13.
13. Handoko ML, de Man FS, Happe CM, Schalij I, Musters RJ, Westerhof N, et al. Opposite effects of training in rats with stable and progressive pulmonary hypertension. Circulation. 2009;120:42–9.
14. Black SM, Nozik-Grayck E. Compartmentalization of redox-regulated signaling in the pulmonary circulation. Antioxid Redox Signal. 2019;31:801–3.
15. Legchenko E, Chouvarine P, Borchert P, Fernandez-Gonzalez A, Snay E, Meier M, et al. PPARγ agonist pioglitazone reverses pulmonary hypertension and prevents right heart failure via fatty acid oxidation. Sci Transl Med. 2018;10:eaao0303.
16. Meng XW, He CX, Chen X, Yang XS, Liu C. The extract of Gnaphalium affine D. Don protects against H2O2-induced apoptosis by targeting PI3K/AKT/GSK-3beta signaling pathway in cardiomyocytes. J Ethnopharmacol. 2020;268:113579.
17. Specht K, Kant S, Addington A, McMillan R, Hulver M, Learnard H, et al. Nox4 mediates skeletal muscle metabolic responses to exercise. Mol Metab. 2021;45:101160.
18. Meng XM, Ren GL, Gao L, Yang Q, Li HD, Wu WF, et al. NADPH oxidase 4 promotes cisplatin-induced acute kidney injury via ROS-mediated programmed cell death and inflammation. Lab Invest. 2018;98:63–78.
19. Chen Y, Yuan T, Zhang H, Yan Y, Wang D, Fang L, et al. Activation of Nrf2 attenuates pulmonary vascular remodeling via inhibiting endothelial-to-mesenchymal transition: an insight from a plant polyphenol. Int J Biol Sci. 2017;13:1067–81.
20. Xu J, Li H, Irwin MG, Xia ZY, Mao X, Lei S, et al. Propofol ameliorates hyperglycemia-induced cardiac hypertrophy and dysfunction via heme oxygenase-1/signal transducer and activator of transcription 3 signaling pathway in rats. Crit Care Med. 2014;42:e583–94.
21. Li H, Lu W, Cai WW, Wang PJ, Zhang N, Yu CP, et al. Telmisartan attenuates monocrotaline-induced pulmonary artery endothelial dysfunction through a PPAR gamma-dependent PI3K/Akt/eNOS pathway. Pulm Pharmacol Ther. 2014;28:17–24.
22. Yuan T, Zhang H, Chen D, Chen Y, Lyu Y, Fang L, et al. Puerarin protects pulmonary arteries from hypoxic injury through the BMPRII and PPARgamma signaling pathways in endothelial cells. Pharmacol Rep. 2019;71:855–61.
23. Fan F, He J, Su H, Zhang H, Wang H, Dong Q, et al. Tribbles homolog 3-mediated vascular insulin resistance contributes to hypoxic pulmonary hypertension in intermittent hypoxia rat model. Front Physiol. 2020;11:542146.
24. Zhang S, Liu J, Zheng K, Chen L, Sun Y, Yao Z, et al. Exosomal miR-211 contributes to pulmonary hypertension via attenuating CaMK1/PPAR-gammaaxis. Vascul Pharmacol 2020;136:106820.
25. Kang BY, Park KK, Kleinhenz JM, Murphy TC, Green DE, Bijli KM, et al. Peroxisome proliferator-activated receptor gamma and microRNA 98 in hypoxia-induced endothelin-1 signaling. Am J Respir Cell Mol Biol. 2016;54:136–46.
26. Zhaorigetu S, Bair H, Jin D, Gupta VS, Pandit LM, Bryan RM, et al. Extracellular vesicles attenuate nitrofen-mediated human pulmonary artery endothelial dysfunction: implications for congenital diaphragmatic hernia. Stem Cells Dev. 2020;29:967–80.
27. Yao L, Lu P, Li Y, Yang L, Feng H, Huang Y, et al. Osthole relaxes pulmonary arteries through endothelial phosphatidylinositol 3-kinase/Akt-eNOS-NO signaling pathway in rats. Eur J Pharmacol. 2013;699:23–32.
28. Jama HA, Muralitharan RR, Xu C, O'Donnell J, Bertagnolli M, Broughton B, et al. Rodent models of hypertension. Br J Pharmacol. 2021. https://doi.org/10.1111/bph.15650.
29. Hennigs JK, Cao A, Li CG, Shi M, Mienert J, Miyagawa K, et al. PPARgamma-p53-mediated vasculoregenerative program to reverse pulmonary hypertension. Circ Res. 2021;128:401–18.
30. Gomez-Arroyo JG, Farkas L, Alhussaini AA, Farkas D, Kraskauskas D, Voelkel NF, et al. The monocrotaline model of pulmonary hypertension in perspective. Am J Physiol Lung Cell Mol Physiol. 2012;302:L363–9.
31. Hill NS, Gillespie MN, McMurtry IF. Fifty Years of Monocrotaline-induced pulmonary hypertension: what has it meant to the field? Chest. 2017;152:1106–8.
32. Jain PP, Zhao T, Xiong M, Song S, Lai N, Zheng Q, et al. Halofuginone, a promising drug for treatment of pulmonary hypertension. Br J Pharmacol. 2021;178:3373–94.
33. Kuwabara Y, Tanaka-Ishikawa M, Abe K, Hirano M, Hirooka Y, Tsutsui H, et al. Proteinase-activated receptor 1 antagonism ameliorates experimental pulmonary hypertension. Cardiovasc Res. 2019;115:1357–68.
34. Shimizu T, Higashijima Y, Kanki Y, Nakaki R, Kawamura T, Urade Y, et al. PERK inhibition attenuates vascular remodeling in pulmonary arterial hypertension caused by BMPR2 mutation. Sci Signal. 2021;14:eabb3616.
35. Hansmann G, Calvier L, Risbano MG, Chan SY. Activation of the metabolic master regulator PPARgamma: a potential PIOneering therapy for pulmonary arterial hypertension. Am J Respir Cell Mol Biol. 2020;62:143–56.
36. Wolf D, Tseng N, Seedorf G, Roe G, Abman SH, Gien J. Endothelin-1 decreases endothelial PPARgamma signaling and impairs angiogenesis after chronic intrauterine pulmonary hypertension. Am J Physiol Lung Cell Mol Physiol. 2014;306:L361–71.
37. Tseng V, Sutliff RL, Hart CM. Redox biology of peroxisome proliferator-activated receptor-gamma in pulmonary hypertension. Antioxid Redox Signal. 2019;31:874–97.
38. Bi R, Bao C, Jiang L, Liu H, Yang Y, Mei J, et al. MicroRNA-27b plays a role in pulmonary arterial hypertension by modulating peroxisome proliferator-activated receptor gamma dependent Hsp90-eNOS signaling and nitric oxide production. Biochem Biophys Res Commun. 2015;460:469–75.
39. Peng X, Chen R, Wu Y, Huang B, Tang C, Chen J, et al. PPARgamma-PI3K/AKT-NO signal pathway is involved in cardiomyocyte hypertrophy induced by high glucose and insulin. J Diabetes Complications. 2015;29:755–60.
40. Liu X, Zhang S, Wang X, Wang Y, Song J, Sun C, et al. Endothelial cell-derived SO controls wndothelial cell inflammation, smooth muscle cell proliferation, and collagen synthesis to inhibit hypoxic pulmonary vascular remodelling. Oxid Med Cell Longev. 2021;2021:5577634.
41. Kang B, Park K, Kleinhenz J, Murphy T, Green D, Bijli K, et al. Peroxisome proliferator-activated receptor γ and microRNA 98 in hypoxia-induced endothelin-1 signaling. Am J Respir Cell Mol Biol. 2016;54:136–46.
42. Daneva Z, Marziano C, Ottolini M, Chen Y, Baker T, Kuppusamy M, et al. Caveolar peroxynitrite formation impairs endothelial TRPV4 channels and elevates pulmonary arterial pressure in pulmonary hypertension. Proc Natl Acad Sci USA. 2021;118:e2023130118.
43. Boehm M, Tian X, Ali M, Mao Y, Ichimura K, Zhao M, et al. Improving right ventricular function by increasing BMP signaling with FK506. Am J Respir Cell Mol Biol. 2021;65:272–87.
44. Ambade A, Hassoun P, Damico R. Basement membrane extracellular matrix proteins in pulmonary vascular and right ventricular remodeling in pulmonary hypertension. Am J Respir Cell Mol Biol. 2021;65:245–58.
45. Potus F, Ruffenach G, Dahou A, Thebault C, Breuils-Bonnet S, Tremblay È, et al. Downregulation of microRNA-126 contributes to the failing right ventricle in pulmonary arterial hypertension. Circulation. 2015;132:932–43.
46. Leopold J, Kawut S, Aldred M, Archer S, Benza R, Bristow M, et al. Diagnosis and treatment of right heart failure in pulmonary vascular diseases: a national heart, lung, and blood institute workshop. Circulation. 2021;14:e007975.
47. Tajsic T, Morrell N. Smooth muscle cell hypertrophy, proliferation, migration and apoptosis in pulmonary hypertension. Compr Physiol. 2011;1:295–317.
48. Feng F, Harper R, Reynolds P. BMPR2 gene delivery reduces mutation-related PAH and counteracts TGF-β-mediated pulmonary cell signalling. Respirology. 2016;21:526–32.
49. Wallace E, Morrell N, Yang X, Long L, Stevens H, Nilsen M, et al. A Sex-specific microRNA-96/5-hydroxytryptamine 1B axis influences development of pulmonary hypertension. Am J Respir Crit Care Med. 2015;191:1432–42.

50. Hood K, Mair K, Harvey A, Montezano A, Touyz R, MacLean M. Serotonin signaling through the 5-HT receptor and NADPH Oxidase 1 in pulmonary arterial hypertension. Arterioscler Thromb Vasc Biol. 2017;37:1361–70.
51. Adesina S, Wade B, Bijli K, Kang B, Williams C, Ma J, et al. Hypoxia inhibits expression and function of mitochondrial thioredoxin 2 to promote pulmonary hypertension. Am J Physiol Lung Cell Mol Physiol. 2017;312:L599–L608.
52. Zhang X, Liu Q, Zhang C, Sheng J, Li S, Li W, et al. Puerarin prevents progression of experimental hypoxia-induced pulmonary hypertension via inhibition of autophagy. J Pharmacol Sci. 2019;141:97–105.
53. Gomez-Puerto M, van Zuijen I, Huang C, Szulcek R, Pan X, van Dinther M, et al. Autophagy contributes to BMP type 2 receptor degradation and development of pulmonary arterial hypertension. J Pathol. 2019;249:356–67.